RESEARCH PAPER

PCCP
www.rsc.org/pccp

Assessment of theoretical prediction of the NMR shielding tensor of $^{195}PtCl_xBr_{6-x}^{2-}$ complexes by DFT calculations: experimental and computational results†

Emmanuel Penka Fowe,[a] Peter Belser,[a] Claude Daul[a] and Henry Chermette*[b]

[a] *Département de Chimie, Université de Fribourg, chemin du Musée 9, CH-1700 Fribourg, Switzerland*

[b] *Laboratoire de Chimie Physique Théorique, Université Claude Bernard Lyon-1 and UMR CNRS 5182, bât 210, 43 bd du 11 novembre 1918, F-69622 Villeurbanne Cedex, France. E-mail: henry.chermette@univ-lyon1.frcherm@in2p3.fr*

Received 13th January 2005, Accepted 7th March 2005
First published as an Advance Article on the web 17th March 2005

In the present work, the ZORA spin–orbit Hamiltonian, in conjunction with the gauge including orbital (GIAO) method based on DFT theory has been used to calculate ^{195}Pt chemical shift of $^{195}PtCl_xBr_{6-x}^{2-}$ complexes. Excellent agreement with experiments has been obtained for calculations bearing on optimized geometries and all electrons triple zeta + polarization (TZP) STO basis sets: the relative error with respect to experiment amounts to $<1.5\%$. It is found that the Pt chemical shift is dominated by the paramagnetic and the spin orbit contribution, whereas the diamagnetic term remains negligible. The influence of the quality of the basis sets has been studied and found to be small, provided a basis set like TZP is used. Several calculations have been performed in order to establish the sensitivity of the chemical shift to a variation in the bond lengths. A strong dependence has been found, with an increase of the chemical shift amounting to 150 ppm pm^{-1} for a distance decrease. Large sensitivity to the solvation, leading to changes in the structure, is then expected. Different tests using conductor-like screening models have been performed in order to establish the sensitivity of the chemical shift to solvation. It has been observed that the changes in the geometry are more important than charge transfers. Finally, the sensitivity of the system to the exchange–correlation functional is found rather weak, at least among the GGA functionals.

Introduction

The first experimental measurements of the chemical shifts in Pt halides were reported in 1968 by von Zelewsky.[1] He observed that mixed platinum halides exhibit strong chemical shifts. The same year Dean[2] and Green published the first predictions of platinum chemical shift. For the first time Ramsey equations[3] were used for calculation of the paramagnetic tensor known to be the major contribution of the shielding tensor in PtX_4 planar square complexes, showing that the orbital energy gap contributed to the platinum chemical shift less than did the covalence of the platinum–ligand bonds.

These pioneer calculations on platinum have been of limited use for a while, because of the high number of electrons in platinum, involving a large amount of computer time and requiring relativistic corrections to be taken into account. In order to reduce the computational demand of such systems, Kaupp *et al.*[4] have for the first time proposed a DFT approach involving the use of pseudo potentials for the representation of the electronic core of transition metals.

Indeed, the breakthrough in the calculation of the NMR chemical shift can be related to the work of Malkin *et al.*[5] who were the first to compute this property through a DFT approach with Kohn–Sham independent gauge for localized orbitals (IGLO).[6] Later, a significant development in the computation of the chemical shift has been brought by the works of Schreckenbach[7a,b,8] where the calculation of NMR shielding tensors using gauge including atomic orbitals (GIAO) and modern density functional theory has been applied to calculate ^{17}O absolute shielding in transition metal oxides $[MO_4]^{n-}$. This model has also successfully been used by Gilbert to calculate the ^{195}Pt chemical shift for a series of Pt(II) complexes.[9]

Finally, for the sake of completeness, we will also mention that Pickard and Mauri[10] have extended the Blöchl[11] projector augmented wave (PAW) in order to include the gauge, leading to calculations of the NMR chemical shifts with pseudo potentials. Their gauge-including projector augmented wave (GIPAW) permits to calculate NMR chemical shifts with a pseudopotential approach leading to results comparable to GIAO all electron calculations.

Experimental details

^{195}Pt is a nucleus with 1/2 spin and an isotopic abundance of 33.7% well suitable for NMR experiments. In the practical experiments,[12] measurements of the peak area are performed, corresponding to an aqueous solution of 1 mol L^{-1} Na_2PtCl_6 concentration in which a 1.5 mol solution of sodium bromide is added. A substitution of chlorine by bromine in the complex follows, leading to different peaks in the spectrum. NMR experiments were performed with a Bruker 300 MHz apparatus, at room temperature.

The change in the chemical environment around platinum leads to the observation of different peaks with quasi constant

† Electronic supplementary information (ESI) available: Contributions to the paramagnetic isotropic and the spin–orbit (Fermi contact) isotropic NMR shielding (Table S1); relative energies (eV) of frontier orbitals with respect to the HOMO for $PtCl_6^{2-}$ and $PtBr_6^{2-}$ complexes (Table S2). See http://www.rsc.org/suppdata/cp/b5/b500574d/

DOI: 10.1039/b500574d

intervals, as reported in Table 3. The solution will contain some isomers, such as *cis* and *trans* $[PtCl_4Br_2]^{2-}$; in that case, the abundance related to these isomers (4/5 for the *cis* form) enables to differentiate them through the observation of the integrals of the peaks on the spectrum for a shift amounting 582–583 ppm: these integrals amounting to 128.2 and 31.6 correspond to a ratio of 0.80/0.19, in agreement with the theoretical prediction.

Theoretical details

Frozen core approximation

As indicated below, the calculations have been performed with ADF code[13] which uses Slater-type orbitals as basis functions. The frozen core approximation has been retained for the geometry optimization of the complexes. This approximation assumes that molecular orbitals (MOs) describing inner shell electrons remain unperturbed in going from a free atom to a molecule. Thus, these inner electrons can be excluded from the variational procedure and, instead, be pre-calculated in an atomic calculation and kept frozen thereafter. The justification for this approximation is that the inner-shell electrons of an atom are less sensitive to their environment than are the valence electrons. This approximation, widely used by ADF users, has been proved to (efficiently) lead to a structure extremely close to those obtained through all electron calculations. In the present work, this will be once more checked and verified, provided one takes care of the numerical accuracy which is more critical in all electron calculations.

On the contrary, for the calculation of the shielding tensor (*vide infra*), it is necessary to take into account any change in all orbitals, including core orbitals which, being localised near the nuclei, are strongly interacting with the nuclear spin momentum. We have, therefore, calculated the shielding tensor with all electrons basis sets, and also performed calculations with frozen cores, in order to evaluate the contribution of core orbitals to the evaluation of the chemical shift.

Relativistic ZORA approximation

The ZORA approximation is readily derived from the relativistic time-independent single-particle Dirac equation for an electron in external magnetic field **B**:

$$\begin{pmatrix} V(r) & c\sigma\pi \\ c\sigma\pi & V(r)-2c^2 \end{pmatrix}\begin{pmatrix} |\phi\rangle \\ |\chi\rangle \end{pmatrix} = E\begin{pmatrix} |\phi\rangle \\ |\chi\rangle \end{pmatrix} \qquad (1)$$

where σ are the Pauli spin matrices, E is the total energy, c is the speed of light, π is the canonical momentum operator given by $\pi = \mathbf{p} + (1/c)\mathbf{A}(\mathbf{r})$ with $\mathbf{B} = \mathbf{rot}\ \mathbf{A}(\mathbf{r})$.

$V(r)$ is the sum of the nuclear, Hartree and exchange–correlation potential, corresponding to the effective Kohn–Sham potential, and $|\phi\rangle$ and $|\chi\rangle$ are, respectively, the large and small components of the Dirac wave function related by $|\chi\rangle = X|\phi\rangle$, where

$$X = \frac{1}{2c}\left(1 + \frac{E - V(r)}{2c^2}\right)^{-1}\sigma\pi \qquad (2)$$

It is therefore possible to express eqn. (1) in terms of the large component (that needs to be normalized) of the wave function only

$$(V(r) + c\sigma\ \pi X)|\phi\rangle = E|\phi\rangle \qquad (3)$$

To avoid the divergence problem of the Coulomb potential for the region close to the nucleus, eqn. (2) has been rewritten[14] as follows:

$$X = \left(\frac{c}{2c^2 - V(r)}\right)\left(1 + \frac{E}{2c^2 - V(r)}\right)^{-1}\sigma\pi \qquad (4)$$

Then, if we consider that $E \lll (2c^2 - V(r))$ and develop to zeroth order in $E/(2c^2 - V(r))$, we obtain the so-called zero-order regular approximation (ZORA[15a,b]) which remains valid close to the nucleus where the Coulomb potential is divergent.

Within these approximations, the Hamiltonian takes the form:

$$H^0 = V + \vec{\boldsymbol{p}}\frac{c^2}{2c^2 - V}\vec{\boldsymbol{p}} + \frac{c^2}{2c^2 - V}\vec{\boldsymbol{\sigma}}\cdot(\vec{\nabla}V \times \vec{\boldsymbol{p}}) \qquad (5)$$

The ZORA approximation provides the possibility to perform all electron calculations. ZORA can further be approximated by neglecting the last term (*i.e.* spin–orbit interaction) in eqn. (5). This is called scalar relativistic corrections, since only the spin–orbit term splits/couples non-relativistic representations. The scalar ZORA has been used in this work for geometry optimization.

Nuclear shielding tensor

Using atomic units, the shielding tensor[16] for a given nucleus is defined as the second derivative of the total electronic energy, E, with respect to a constant external magnetic field, B, and a nuclear magnetic moment of nucleus with the tth component μ_t

$$\begin{aligned}\sigma_{st} &= \left.\frac{\partial^2 E}{\partial B_S \partial \mu_t}\right|_{\vec{\boldsymbol{B}}=\vec{\boldsymbol{\mu}}=0} \\ &= \frac{\partial}{\partial B_S}\left\langle \Psi(\vec{\boldsymbol{B}})\middle| h_t^{01} + \sum_{r=1}^{3} B_r h_{rt}^{11}\middle|\Psi(\vec{\boldsymbol{B}})\right\rangle_{\vec{\boldsymbol{B}}=0}\end{aligned} \qquad (6)$$

$\Psi(\vec{\boldsymbol{B}})$ represents the ground state electronic eigenfunction under the influence of the external magnetic field. s,t refer to the tensor components.

As detailed in ref. 7a and 7b, expression (6) can be split into paramagnetic, diamagnetic and spin–orbit contributions:

$$\sigma_{st} = \sigma_{st}^{\ p} + \sigma_{st}^{\ d} + \sigma_{st}^{\ so} \qquad (7)$$

Chemical shift

The chemical shift is simply evaluated as

$$\delta(\text{sample}) = \sigma(\text{ref}) - \sigma(\text{sample}) \qquad (8)$$

In the present work, the $PtCl_6^{2-}$ has been retained as a reference sample.

Computational details

The geometry optimization has been carried out for an isolated cluster and, for some complexes, in solvent media, using the ADF 2000 and 2002 packages.[13]

The ZORA TZP basis set with frozen core on Pt (4d), Br (3p), and Cl (2p) has been used. ZORA relativistic corrections have been applied, (scalar in geometry optimizations and with spin–orbit for the calculation of the shielding tensor). LDA exchange–correlation functional (Slater for exchange[17] and Vosko–Wilk–Nusair for correlation[18]) has been retained for the geometry optimization. This is justified by the fact that the geometries obtained are closer to the experiment than the generalized gradient approximations (GGA) let obtain.[19] Indeed, one obtains trends for the properties calculated at the GGA level of approximation (or hybrid functionals) on such geometries which are similar to those calculated at self-consistent GGA geometries.

The solvation model retained for the study of solvent effects is the "conductor-like screening model" (COSMO) model. It is well known that dielectric screening energies of a given geometry scale as $(\varepsilon - 1)(\varepsilon + 1)$ where ε is the permittivity of the screening medium and x is a parameter in the range 0–2 (for water $\varepsilon = 78.8$ and $x = 0$).

In reality, for a conductor $\varepsilon \rightarrow \infty$, and screening in a conductor can be handled easily. The total screening energy is classically given by the following expression using the image charge method[20]

$$\Delta E = -1/2QDQ \qquad (9)$$

where $D_{ij} = R/(R^2 - r_i r_j)^2$, and if the solvent effect is taken into account, the total energy of the conductor-like system is given as

$$E = 1/2QCQ + QBq + 1/2qAq \qquad (10)$$

where Q is a vector containing n point charges Q_i at position r_i within a sphere of radius R. Q_i is supposed to be enveloped by an arbitrary surface S and the screening energy can be obtained by dividing Q_i into m small segment surfaces s with constant charge density and corresponding point charge q_i.

B (m*n matrix) is the electrostatic interaction of unit charges at r_j with unit charges on s.

C is the classical coulomb operator between the charges Q_i.

A (m*m) is the electrostatic interaction of two different surface charge q_i.

Therefore, by minimizing eqn. (10), we can obtain the effective screening charge

$$q^* = -A^{-1}BQ = DQ. \qquad (11)$$

and by implementing (11) into (10), the total energy of the screened system becomes

$$E(\sigma^*) = -1/2Q(C - BA^{-1}B)Q \cong -1/2QD^*Q \qquad (12)$$

This equation is similar for the total screening energy of a conductor [eqn. (9)].

During the computational process, we can choose to include D^* in the Hamiltonian of the system as a perturbation (post-SCF calculation, named model 1) or during the SCF procedure (Variation method, named model 2), so that we have compared the efficiency of both models.

Three different types of cavity[21] used to represent sphere surface model of the solute molecule in the solvent have been compared in the present work. These surfaces are constructed with the GEPOL93 algorithm.[22] *Asurf* yields the solvent accessible surface (SAS), it consists of the path traced by the center of a spherical solvent molecule rolling on the van der Waals surface. *Esurf* gives the solvent excluding surface (SES), which consists of the path traced by the surface of a spherical solvent molecule rolling on the VDW surface. *Klamt* as well as *Esurf* excludes also the cusp regions of the overlapping van der Waals spheres, but differs in the formulation.

Since we do not have experimental values to compare with, the influence of solvent—namely water-effect—has been computed only for $[PtCl_6]^{2-}$ and $[PtBr_6]^{2-}$ complexes for which, because of their O_h symmetry, only bond lengths can be altered. No angular distortion, nor any differential (Br *vs.* Cl) charge transfer can be expected for the inclusion of these complexes into the solvent model.

The ^{195}Pt chemical shift has been estimated using the NMR program implemented in ADF using the wave function calculated with the ZORA relativistic approximation and including spin–orbit term. We have distinguished calculations performed with frozen cores and all electron calculations on ^{195}Pt.

Table 1 Geometries used to compute the chemical shift: calculations performed with the scalar relativistic ZORA approximation, triple zeta + polarization basis set (TZP), and LDA approximation

System	Geometry	Pt–Cl bond length	Pt–Br bond length
$[PtCl_6]^{2-}$	Optimized	2.341	
	Experiment[29]	2.317–2.334	
$[PtCl_5Br]^{2-}$	Optimized	2.341	2.484
trans $[PtCl_4Br_2]^{2-}$	Optimized	2.340	2.489
cis $[PtCl_4Br_2]^{2-}$	Optimized	2.334	2.488
	Experiment[30]	2.358	2.471
Meridian $[PtCl_3Br_3]^{2-}$	Optimized	2.345	2.489
Facial $[PtCl_3Br_3]^{2-}$	Optimized	2.345	2.486
trans $[PtCl_2Br_4]^{2-}$	Optimized	2.334	2.489
cis $[PtCl_2Br_4]^{2-}$	Optimized	2.344	2.489
$[PtClBr_5]^{2-}$	Optimized	2.344	2.489
$[PtBr_6]^{2-}$	Optimized		2.488

[a] Gas electronic diffraction, ref. 23. [b] ref. 24.

Results and discussion

1. Structure of the $^{195}PtCl_xBr_{6-x}{}^{2-}$ complexes

Table 1 gives the geometries used to compute the chemical shift.

Since the NMR experiments are performed in solution, no accurate comparison between the experimental structure and theoretical ones (charged gas phase cluster) can be made; however, the comparison with solid-state structure, when available, indicates a rather good agreement with the theoretical structure obtained at the LDA level of approximation.

Table 2 Influence of the model to compute solvent effect on the structure of the complex

Surface model	Bond length (Model 1)	Partial charge of Pt (Mulliken)	Solvation energy/eV	Bond length (Model 2)	Partial charge of Pt (Mulliken)	Solvation energy/eV
A						
Asurf	2.519	0.6362	−5.6	2.476	0.6653	−5.63
Esurf	2.525	0.6313	−6.7	2.472	0.5545	−7.19
Klamt	2.524	0.6333	−6.27	2.466	0.6056	−6.47
B						
Asurf	2.342	0.6018	−5.83	2.330	0.5907	−5.85
Esurf	2.340	0.6041	−7.39	2.326	0.4330	−7.67
Klamt	2.340	0.6046	−6.9	2.320	0.5511	−7.0

A – Averaged Pt–Br bond length (Å) in $[PtBr_6]^{2-}$ complexes, (gas phase length: Pt–Br: 2.487 (Å); B – Averaged Pt–Cl bond length (Å) in $[PtCl6]^{2-}$ complexes, (gas phase length: Pt–Cl: 2.341 (Å).

2. Solvent effects on the structure

Table 2 gathers the results of the solvation effects as calculated through the 3 models, and the two models of solvation.

The bond length reported for the solvated complexes is an average of the six lengths obtained through the optimization process: this takes its origin in the fact that the excluding or accessible surface used in the solvation models does not retain the symmetry of the system, allowing a slight distortion to occur. It is interesting to notice that model 2 leads in all models to shorter bond lengths, *ca.* 10 to 21 pm, according to the model retained. The change in Mulliken charges, on the contrary, is rather small with the *Asurf* model, a little bit larger with the *Esurf* model, and roughly in-between with the *Klamt* model (the platinum charge decreases through solvation by 0.05 for $PtCl_6^{2-}$, and 0.03 for $PtBr_6^{2-}$). This is related to the solvation energies which are, for the *Klamt* model, between the *Asurf* model (smaller) and the *Esurf* model (larger).

On the contrary, model 1, which does not permit a change in the ionicity of the Pt–X bonds through a relaxation process, is less sensitive and leads to distortions in the opposite direction, if any. One should not exclude sensitivity of the effect to the basis set, which has not been studied.

3. NMR chemical shifts of the $^{195}PtCl_xBr_{6-x}^{2-}$ complexes

The $[PtCl_6]^{2-}$ complex has been used as a reference for the chemical shift. As can be seen in Table 3, a very good agreement with experiment is obtained provided that the shielding tensor is computed with an all-electron basis set; PW91[23] gradient corrections have been used for exchange and correlation. On the contrary, the calculations with frozen cores exhibit a systematic deviation, which was expected because of the participation of core levels to the shielding which cannot be taken into account. One should note that the chemical shift is dominated by the paramagnetic contribution whereas the diamagnetic contribution is rather small (0.5%).

The paramagnetic chemical shift is largely determined by the first order coupling magnetic coupling term between occupied and virtual orbitals. Table 3 indicates also that as the number of softer ligands (Br) increases, through substitution of the harder ones (Cl), the chemical shift becomes more and more negative.

The necessity to perform all electron calculations is clearly visible and, as already said, was expected.

The chemical shift is roughly proportional to the number of bromine atoms, as can be seen by inspection of Fig. 1 and from Table 3. The assignment of the chemical shift to each isomer is experimentally straightforward because it can be extracted from the relative intensity of the peaks which is given by the statistical distribution of the isomers (*e.g.* PtX_4Y_2 exists with a theoretical ratio *cis*/*trans* = 4).

Fig. 1 shows an excellent correlation between the computed and experimental values, the absolute maximum deviation being $<2.3\%$, obtained for $[PtBr_6]^{2-}$, with the absolute average deviation being $<1.5\%$.

In order to check what could be the origin of this (small) deviation, we have calculated the influence of the bond length on the chemical shift. This is easy to perform on the $[PtBr_6]^{2-}$ complex because, thanks to its O_h symmetry, there is only one bond length parameter. Fig. 2 shows that one gets a quasi-linear relationship between the chemical shift and the bond length, with a slope of *ca.* 150 ppm pm^{-1}. A similar, but more modest slope (50 ppm pm^{-1}) was found by Wolff *et al.* for mercury halides.[8] One can notice (Table 3) that the experimental difference in the chemical shift of the different isomers is rather small (1–2 ppm), and found somewhat larger theoretically (10–20 ppm). However the relative order between 2 isomers is always in agreement with the experiment. Finally, one has to recall that the chemical shift depends strongly on the geometry accuracy, the 1 ppm difference in two chemical shifts corresponding to a difference of 0.01 pm, *i.e.* much less than the precision required for usual geometry optimization computation.

In other words, whereas the accuracy of the calculated structures may be less than 0.1 pm, because of the quality of the basis sets, or perhaps the effect of the frozen core approximation, or the approximations in the Hamiltonian, the precision for the chemical shift is found higher and is related to the facts that the same approximations apply similarly to all atoms, the coordination number of the platinum as well as its oxidation degree is unchanged between the different complexes, *etc.*

For the sake of completeness, we have re-optimized the geometry of all complexes with different basis sets, and the corresponding errors in the chemical shifts are reported in Table 4. The optimization criteria were fixed to a rather high accuracy, such as 10^{-4} E_h pm^{-1} for the energy gradient, 0.01 pm in bond length, and a numerical accuracy (accint) for integrals equal to 10. The basis sets were all electron TZP, TZ2P and QZP. The quasi-linear trend amongst the 10 compounds has been retrieved, with an averaged deviation amounting −29, −38, and +32 for TZP, TZ2P and QZP, respectively. Significantly, the deviation increases with the number of bromine atoms in the complex, roughly proportionally to the number of Br–Br nearest neighbours. This could be reasonably assigned to a kind of basis set superposition error dominated by the bromine basis set. In any case, this shows that the all-electron TZP basis set is large enough to provide totally significant trends in the chemical shift among the isomers.

It is indeed interesting to compare the importance of the contributions to the isotropic NMR shielding, coming from orbital excitations either in the paramagnetic isotropic term

Table 3 Different contributions (paramagnetic, diamagnetic, spin–orbit/Fermi contact (SO/FC) to the ^{195}Pt NMR chemical shift (ZORA formalism with all-electron TZP basis sets). Values are given in ppm. Values obtained with the frozen cores approximation are in parentheses. diff = $\delta_{cal} - \delta_{exp}$

Compound	δ param	δ diamag	δ SO/FC	δ calculated	δ exp	Diff
$[PtCl_6]^{2-}$	0 (0)	0 (0)	0 (0)	0 (0)	0	0 (0)
$[PtCl_5Br]^{2-}$	−166.7(−122.7)	0.6(0.7)	−110.7(−80.3)	−276.8(−202.4)	−282	5.2(79.6)
trans-$[PtCl_4Br_2]^{2-}$	−326.4(−241.7)	1.2(1.4)	−258(−187.1)	−583.3(−427.5)	−583.6	0.3(156.1)
cis-$[PtCl_4Br_2]^{2-}$	−344.(−253.7)	1.2(1.4)	−222.8(−162.2)	−565.6(−414.5)	−582.4	16.8(167.9)
Facial$[PtCl_3Br_3]^{2-}$	−531.0(−392.2)	1.8(2.1)	−336.6(−245.8)	−865.8(−636.0)	−889.2	23.4(253.2)
Meridian$[PtCl_3Br_3]^{2-}$	−516.5(−383.0)	1.8(2.1)	−372.6(−271.2)	−887.6(−652.1)	−891.4	3.8(239.2)
trans-$[PtCl_2Br_4]^{2-}$	−699.5(−520.6)	2.4(2.8)	−526.1(−383.3)	−1223.3(−901.2)	−1210	−13.3(308.8)
cis$[PtCl_2Br_4]^{2-}$	−714.3(−530.1)	2.4(2.8)	−489.3(−357.5)	−1201.2(−884.9)	−1210	8.8(325.1)
$[PtClBr_5]^{2-}$	−908.3(−677.2)	3.0(3.5)	−645.6(−472.5)	−1551.7(−1146.2)	−1540	−11.5(393.8)
$[PtBr_6]^{2-}$	−1113.5(−833.5)	3.6(4.2)	−805.4(−590.9)	−1915.2 (−1420.2)	−1870	−45.2(449.8)

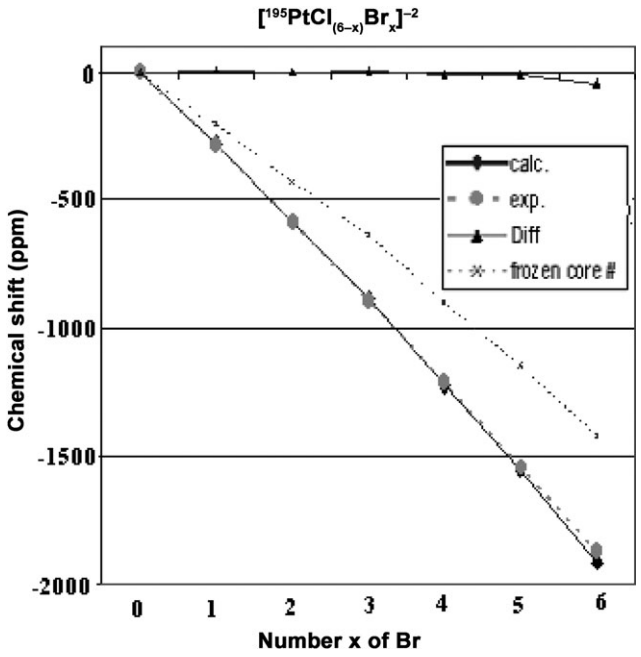

Fig. 1 Variation of the chemical shift with the number of bromide ions in $[^{195}Pt\ Cl_{6-x}Br_x]^{2-}$ complex.

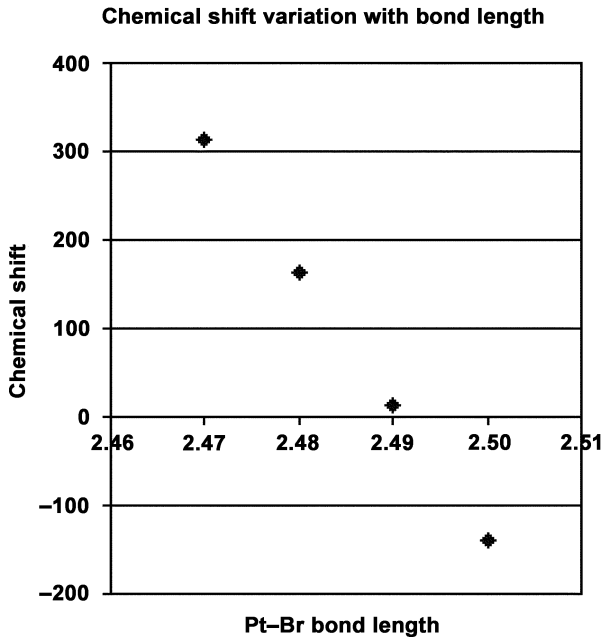

Fig. 2 Variation of the chemical shift (ppm) with the Pt–Br bond length (Å) in $[PtBr_6]^{2-}$.

or the spin–orbit (Fermi contact) term. One can see in Supplementary Table S1† that roughly 2/3 of the effect originates from the paramagnetic contribution. Whereas the diamagnetic contribution to the screening tensor is rather large, it does not involve the virtual orbitals. Accordingly, it is not sensitive to the gap and remains unchanged among the different clusters, therefore not contributing significantly to the chemical shift.

4. Solvent effects on the NMR chemical shift

Because the experiments are performed in aqueous solution, one can expect that it is necessary to take solvent effects into account. As already said, we have restricted this study to the $[PtCl_6]^{2-}$ (reference) and to the $[PtBr_6]^{2-}$ cases, conserving the octahedral symmetry of the complexes. Other molecules would exhibit distortions which may involve different polarizabilities of the Pt–Br and Pt–Cl bonds, and therefore possibly be more sensitive to other parameters such as basis sets.

We have reported in Table 5 the results obtained for the different cavity models, and the perturbational/SCF calculations.

The results show unambiguously that it is necessary to use a variational process for the calculation of solvent effects, namely model 2. This suggests that the charge borne by the complex involves a strong interaction with the solvent, which cannot be accurately approximated by a perturbation treatment. Finally, no test has been performed in order to check if the triangulation of the van der Waals spheres uses a sufficient number of sections. It is fixed to 5 in the ADF code, and is assumed to be accurate enough by the developers.[24] From this table, it appears that the Klamt model provides the best results, as expected on the basis of the general trends derived from other works[25,26]

Table 4 Algebraic deviation (with respect to experiment) of the chemical shift for several basis sets used for the geometry optimizations. The number of Br–Br nearest neighbours is given in parentheses

Basis set system	TZP	TZ2P	QZ4P
$[PtCl_6]^{2-}$ (0)	0	0	0
$[PtCl_5Br]^{2-}$ (0)	−0.3	−7.8	16.4
cis-$[PtCl_4Br_2]^{2-}$ (1)	−5.8	−8.9	30.2
trans-$[PtCl_4Br_2]^{2-}$(0)	−12.4	−23.1	30.2
fac-$[PtCl_3Br_3]^{2-}$ (3)	−21.3	−15.6	26.7
mer-$[PtCl_3Br_3]^{2-}$ (2)	−15.0	−20.6	23.8
cis $[PtCl_2Br_4]^{2-}$ (5)	−19.1	−45.3	35.7
trans $[PtCl_2Br_4]^{2-}$ (4)	−43.3	−60.1	27.5
$[PtClBr_5]^{2-}$ (8)	−50.6	−46.5	16.4
$[PtBr_6]^{2-}$ (12)	−95.9	−119.3	83.9
Average deviation	−29.3	−38.6	32.3

5. Influence of the basis sets and the exchange–correlation functionals

Both of them have been tested. The results obtained indicate that one obtains a very accurate determination of the chemical shift, with an average deviation as small as 0.1% (average absolute deviation less than 1.5%) when a TZP basis set is chosen. This is clearly visible in Fig. 1. Calculations performed with TZ2P basis sets did not lead to any significant improvement brought by the addition of a second polarization function into the basis set. Indeed, slightly worsen results, with an average absolute deviation amounting to 3% have been obtained. This is not too surprising, since on the one hand, the environment of the platinum atom is highly symmetric in the whole set of complexes studied, so that no extra polarization function is needed to describe a (asymmetric) distortion of orbitals. On the other hand it is well known that exchange–correlation functionals lead to optimal descriptions when they are used with large-, but not extra large-basis sets.

Table 5 Solvent effects: deviations of the chemical shift (ppm) for each type of cavity

Surface option	Model 1	Model 2
Asurf	409	−27
ESurf	804	−53
Klamt	523	4

Table 6 Algebraic deviation (with respect to experiment) of the chemical shift for several GGA exchange–correlation functionals

GGA system	PW91	PBE[31]	BLYP[32,33]	OLYP[34,30]	OPBE[28,31]	RevPBE[35]	RPBE[36]
$[PtCl_6]^{2-}$	0	0	0	0	0	0	0
$[PtCl_5Br]^{2-}$	5.2	5.6	−2.8	−7.1	5.	3.1	1.3
trans $[PtCl_4Br_2]^{2-}$	0.3	2.1	−17.5	−22.2	4.1	−2.3	−5.3
cis $[PtCl_4Br_2]^{2-}$	16.8	17.3	1.7	−6.7	17.1	12.4	8.9
Meridian $[PtCl_3Br_3]^{2-}$	23.4	5.4	−21.3	−28.8	8.9	−1	−5.9
Facial $[PtCl_3Br_3]^{2-}$	3.8	23.7	0.2	−10.5	24.7	16.6	11.2
trans $[PtCl_2Br_4]^{2-}$	−13.3	−11.1	−47.9	−54.2	−2.8	−18.8	−25
cis $[PtCl_2Br_4]^{2-}$	8.8	9.7	−23.5	−33.1	15.6	1.5	−5.2
$[PtClBr_5]^{2-}$	−11.7	−0.6	−52.3	−59.8	2.3	−18.7	−26.7
$[PtBr_6]^{2-}$	−45.2	−43.8	−95.6	−100.2	−25.0	−53.6	−63.0

The results obtained with various GGA exchange–correlation functionals belonging to the GGA family are reported in Table 6.

The results show a limited influence on the exchange–correlation functional employed. However, the functionals derived from a combination with a given correlation functional (namely PBE or LYP) are internally consistent, *i.e.* very similar among them. This would indicate that the dynamic correlation, modelled through the correlation functional plays an important role, whereas the exchange functional, which describes the non-dynamical correlation,[27,28] is less important.

Concluding remarks

The uncoupled GIAO-DFT method together with ZORA relativistic corrections have led to an excellent description of the ^{195}Pt NMR spectra of $^{195}PtCl_xBr_{6-x}{}^{2-}$ complexes. The frozen core approximation leads to a deviation of approximately 20%, whereas the full electron calculation provides an agreement with experiment which is extremely good and sensitive to accurate determinations of the bond lengths of the complexes. For this purpose, the triple zeta + polarization (TZP) basis set is sufficient, provided numerical accuracy parameters are severely fixed. These bond lengths are slightly modified by solvation, as expected, and the Klamt model is the one which leads to the best agreement with experiment.

According to eqn. (12) small gap complexes will exhibit a stronger shielding, leading to a larger (negative) chemical shift. This is clearly apparent with the valence eigenvalues pattern of the complexes, reported in Supplementary Table S2.† Since the orbital eigenvalues are dependent on the global charge of a complex (the more negatively charged is a species, the higher in energy—even positive—are the eigenvalues, because of the extra Coulomb repulsion between electrons), Supplementary Table S2 reports the eigenvalues relatively to the HOMO which, in O_h symmetry, involves no central atom orbitals. The $PtCl_6{}^{2-}$ complex is harder, *i.e.* has a larger gap (2 eV) than $PtBr_6{}^{2-}$ (1.5 eV), and all the excitations involving platinum orbitals are higher in energy.

The almost linear dependence on the number of substituted bromide ions will be addressed in more details in a forthcoming publication.

Acknowledgements

This work was supported by the Swiss National Science Foundation and is part of COST Action D26. The CINES is acknowledged for their computer time.

References

1 A. von Zelewsky, *Helv. Chim. Acta*, 1968, **803**.
2 R. R. Dean and J. C. Green, *J. Chem. Soc. A*, 1968, 3047.
3 N. F. Ramsey, *Phys. Rev.*, 1950, **78**, 699.
4 M. Kaupp, V. G. Malkin, O. L. Malkina and D. Salahub, *J. Am. Chem. Soc.*, 1995, **117**, 1851.
5 V. G. Malkin, O. L. Malkina, L. A. Erikson and D. R. Salahub, in *Modern Density Functional Theory: A Tool for Chemistry*, ed. P. Politzer and J. M. Seminario, Elsevier, Amsterdam, 1995, vol. 2.
6 W. Kutzelnigg, U. Fleisher and M. Schindler, in *NMR-Basic Principles and Progress*, Springer-Verlag, Berlin, 1990, vol. 23, p. 165.
7 (*a*) H. G. Schreckenbach and T. Ziegler, *J. Phys. Chem.*, 1995, **99**, 606; (*b*) H. G. Schreckenbach, Relativity and Magnetic Properties. A Density Functional Study, Ph.D. Thesis, University of Calgary, Aberta, Canada, 1996.
8 S. K. Wolff, T. Ziegler, E. van Lenthe and E. J. Baerends, *J. Chem. Phys.*, 1999, **110**, 7689.
9 T. M. Gilbert and T. Ziegler, *J. Phys. Chem. A*, 1999, **103**, 7535.
10 C. J. Pickard and F. Mauri, *Phys. Rev. B*, 2001, **63**, 245101.
11 P. E. Blöchl, *Phys. Rev. B*, 1994, **50**, 17953.
12 A. Hesse, H. Meier and B. Zeeh, *Spektroscopische Methoden in Organische Chemie*, G. Thieme Verlag, Stuttgart, 4th edn., 1991.
13 E. J. Baerends, J. Autschbach, A. Bérces, C. Bo, P. M. Boerrigter, L. Cavallo, D. P. Chong, L. Deng, R. M. Dickson, D. E. Ellis, L. Fan, T. H. Fischer, C. Fonseca Guerra, S. J. A. van Gisbergen, J. A. Groeneveld, O. V. Gritsenko, M. Grüning, F. E. Harris, P. van den Hoek, H. Jacobsen, G. van Kessel, F. Kootstra, E. van Lenthe, D. A. McCormack, V. P. Osinga, S. Patchkovskii, P. H. T. Philipsen, D. Post, C. C. Pye, W. Ravenek, P. Ros, P. R. T. Schipper, G. Schreckenbach, J. G. Snijders, M. Sola, M. Swart, D. Swerhone, G. te Velde, P. Vernooijs, L. Versluis, O. Visser, E. van Wezenbeek, G. Wiesenekker, S. K. Wolff, T. K. Woo and T. Ziegler, ADF2002.03, and ADF2004.01, SCM, Theoretical Chemistry, Vrije Universiteit, Amsterdam, The Netherlands, http://www.scm.com.
14 E. Van Lenthe, Ph.D Thesis, Vrije Universiteit, Amsterdam, 1990.
15 (*a*) E. van Lenthe, E. J. Baerends and J. Snijders, *J. Chem. Phys.*, 1993, **99**, 4597; (*b*) E. van Lenthe, E. J. Baerends and J. Snijders, *J. Chem. Phys.*, 1996, **105**, 6505.
16 H. Fukui, *Magn. Reson. Rev.*, 1987, **11**, 205.
17 J. C Slater, *Phys. Rev.*, 1951, **81**, 385.
18 S. H. Vosko, L. Wilk and M. Nusair, *Can. J. Phys.*, 1980, **58**, 1200.
19 H. Chermette, *Coord. Chem. Rev.*, 1998, **178**, 699.
20 J. D. Jackson, *Classical Electrodynamics*, Wiley, New York, 1975.
21 A. Klamt and G. Schüürmann, *J. Chem. Soc., Perkin Trans. 2*, 1993, **5**, 799.
22 J. Pascual-Ahuir, J. L. E. Silla and I. Tuñon, *J. Comput. Chem.*, 1994, **15**, 1127.
23 J. P. Perdew, J. A. Chevary, S. H. Vosko, K. A. Jackson, M. R. Pederson and D. J. Singh, *Phys. Rev. B*, 1992, **46**, 6671.
24 C. C. Pye and T. Ziegler, *Theor. Chem. Acc.*, 1999, **101**, 396.
25 (*a*) J. Andzelm, C. Kölmel and A. Klamt, *J. Chem. Phys.*, 1995, **103**, 9312; (*b*) A. Klamt, *J. Phys. Chem.*, 1995, **99**, 2224.
26 K. Baldridge and A. Klamt, *J. Chem. Phys.*, 1997, **106**, 6622.
27 (*a*) P. R. T. Schipper, O. V. Gritsenko and E. J. Baerends, *Phys. Rev. A*, 1998, **57**, 1729; (*b*) O. V. Gritsenko, B. Ensing, P. R. T. Schipper and E. J. Baerends, *J. Phys. Chem. A*, 2000, **104**, 8558; (*c*) O. V. Gritsenko, P. R. T. Schipper and E. J. Baerends, *J. Chem. Phys.*, 1997, **107**, 5007.
28 N. C. Handy and A. J. Cohen, *Mol. Phys.*, 2001, **99**, 403.

29 R. Restori and D. Schwarzenbach, *Z. Naturforsch.*, 1993, **A48**, 12.
30 W. Preetz and G. Rimkus, *Z. Naturforsch.*, 1982, **B37**, 1422.
31 J. P. Perdew, K. Burke and M. Ernzerhof, *Phys. Rev. Lett.*, 1996, **77**, 3865.
32 A. D. Becke, *Phys. Rev. A*, 1988, **38**, 3098.
33 C. Lee, W. Yang and R. G. Parr, *Phys. Rev. B*, 1988, **37**, 785.
34 N. C. Handy and A. J. Cohen, *Mol. Phys.*, 2001, **99**, 403.
35 Y. Zhang and W. Yang, *Phys. Rev. Lett.*, 1998, **80**, 890.
36 B. Hammer, L. B. Hansen and J. K. Norskøv, *Phys. Rev. B*, 1999, **59**, 7413.

